






Potential hazards and mitigation of X-ray radiation generated by laser-induced plasma from research-grade laser systems

PHILIP MOSEL,^{1,2} PRANITHA SANKAR,^{1,3} ZULQARNAIN,¹ ELISA APPI,^{1,4}  CHRISTOPH JUSKO,^{1,2} DAVID ZUBER,^{1,3} SVEN KLEINERT,^{1,3}  JAN DÜSING,⁵ JOSE MAPA,¹ GÜNTER DITTMAR,⁶ THOMAS PÜSTER,⁵ PETRA BÖHMER-BRINKS,⁷ JAN-WILLEM VAHLBRUCH,⁸ UWE MORGNER,^{1,3} AND MILUTIN KOVACEV^{1,2,3,*} 

¹Institut für Quantenoptik, Leibniz Universität Hannover, Hannover 30167, Germany

²EXC 2123/1 QuantumFrontiers, Hannover 30167, Germany

³Cluster of Excellence PhoenixD (Photonics, Optics and Engineering – Innovation Across Disciplines), Hannover 30167, Germany

⁴Present address: Department of Physics, Lund University, SE-221 00 Lund, Sweden

⁵Laser Zentrum Hannover e.V., Hannover 30419, Germany

⁶Ingenieur-Büro Prof. Dr.-Ing. G. Dittmar, Aalen 73433, Germany

⁷Leibniz Universität Hannover, Hannover 30167, Germany

⁸Institute of Radioecology and Radiation Protection, Leibniz Universität Hannover, Hannover 30419, Germany

*kovacev@iqo.uni-hannover.de

Abstract: A large range of laser-matter applications employ ultrashort pulses and high laser intensity. Such processes can lead to unrequired X-ray generation, which represents a hazardous radiation factor even for common laboratory research-grade laser systems. We present here an analysis of the radiation dose rate and X-ray spectrum emitted during ablation of a rotating copper cylinder with respect to several laser parameters. The results show that focused sub-picosecond pulses with intensity above 10^{13} W/cm² can exceed the annual irradiation limit even in one hour, requiring appropriate shielding for the safety of the researchers.

© 2022 Optica Publishing Group under the terms of the [Optica Open Access Publishing Agreement](#)

1. Introduction

With the rapid advancement of laser industry, a plethora of high intensity laser systems is emerging all over the world. In particular, femtosecond laser pulses play an ever-expanding role in material processing [1–5], from new product development to high-volume manufacturing, due to the reduced heat-affected area compared to longer pulse duration systems [6,7]. Simultaneously, an ionizing radiation hazard caused by the interaction of laser pulses with peak intensity above 10^{13} W/cm² with solid targets has been steadily observed [8–11]. In the ultrashort regime, the laser pulse energy is rapidly deposited in the target, leading to the ignition of plasma [12,13]. Energetic electrons are ejected from the target, which is responsible for the emission of X-ray radiation by Bremsstrahlung, recombination and line emission [14,15]. These processes are well known and the emission of X-ray radiation in the keV and MeV spectral range from laser-induced plasma is used in different applications [16–21]. However, X-ray emission during laser-material processing leads to a potential health risk, which has been confirmed by previous studies [22–27]. Several laser parameters, such as central wavelength and peak intensity, as well as physical properties of the target, influence the plasma dynamics and consequent X-ray generation [28,29]. Therefore, all these parameters must be taken in consideration with respect to radiation safety. Moreover, in the last decade, the development of high repetition rate laser systems paved the way

for quick, cost-effective laser-material processing [5–7]. However, even in the case of low X-ray dose per pulse, accumulation effects can lead to a total dose rate exceeding the statutory radiation limit which represents a hazardous risk for the operating staff [17,19]. While the investigation of potential radiative hazards during laser micromachining is currently a significant topic for industrial applications, a comparable interest has not been addressed in the scientific research environment. Ultrashort laser systems commonly used in state-of-the-art research laboratories deliver multi-joule pulses with durations down to a few femtoseconds and repetition rates from a few Hz up to several GHz. For strong field nonlinear optics applications, the laser beam is often focused on a target, reaching peak intensities above 10^{13} W/cm². Therefore, the investigation of potentially hazardous X-ray emission from laser-matter interaction is indeed of interest also for the laboratory radiation safety scenario. The recommended annual dose equivalent limit for the general population set by the International Commission on Radiological Protection (ICRP) publication 103 (2007) is 15 mSv/year ($\dot{H}'(3)$) for the eye and 50 mSv/year ($\dot{H}'(0.07)$) for skin and extremities [30]. The latest value can be considered the limit also for laboratory use, since in this case the skin is most likely more exposed to the radiation. This limit results in a maximum dose rate of 25 μ Sv/h ($\dot{H}'(0.07)$) for a non-restricted area during continuous (2000 hours/year) use. However, typically material processing in research involves only short exposure times. By considering an exposure of 50 hours/year, short-term radiation dose values of up to 1000 μ Sv/h ($\dot{H}'(0.07)$) are permissible. Maximum exposure time, minimum working distance and suitable radiation shielding are then essential factors for the protection of experimentalists [31].

In this study, five different research-grade laser systems with intensities between 10^{13} W/cm² and 10^{16} W/cm² are used to induce X-ray emission from a pure, solid copper target. Copper is a material commonly present in optical research laboratories, often used as beam dumps or in crystal holders due to its high thermal conductivity, and therefore represents an interesting target for the investigation of potential radiative hazards. The dose rate and the spectral distribution of the emitted X-ray radiation is analyzed with respect to the laser parameters in order to identify their influence. Moreover, the X-ray emission is also investigated for nonlinear processes which do not exceed the damage threshold of the target, such as the ones that take place inside high-power ultrashort laser systems. The presented results show a clear K_{α} line emission during white-light generation in a YAG crystal, a process commonly used in ultrashort optical-parametric amplifiers. Finally, the shielding properties of different materials are tested and conclusions on the recommended safety practices are presented. Note that, while the plasma's formation and expansion are complex dynamics which require a complete theoretical model for accurate estimations, here experimental measurements are carried out in order to draw a realistic scenario for radiation protection in the laboratory environment.

2. Experimental methods

2.1. Optical setup

In order to perform measurements on X-ray generation, the experimental setup shown in Fig. 1 is used. A laser pulse is focused on a rotatable copper cylindrical sample of 1.8 cm in diameter using a plano-convex lens of 50 mm focal length. The estimated focal diameter is equal to 100 μ m. The rotation speed of the copper cylinder is of 1.5 revolution/second. The target is set at an angle of 45° with respect to the axis of the incident laser beam. The X-ray detector can be placed at different angles in order to study the angular distribution of the generated radiation. Each measurement is integrated over 6 seconds. The spectral emission and dose rate of the generated X-ray radiation are studied for different laser systems, at different working distances, as well as for long material processing times. An overview of the used laser systems, is listed in Table 1. Similar systems and parameters are commonly found in most nonlinear optics laboratories. In particular, two titanium-sapphire based laser systems are used, which deliver femtosecond pulses with a central wavelength of around 800 nm: a commercial chirped pulse amplifier (CPA) system

(Dragon, KMLabs Inc.) and a custom optical parametric chirped-pulse amplifier (OPCPA). In addition, two Ytterbium based systems are employed, which deliver longer pulses with a central wavelength of about 1030 nm: a commercial solid-state amplifier (neoYb, neoLase GmbH) and a home-built solid-state amplifier.

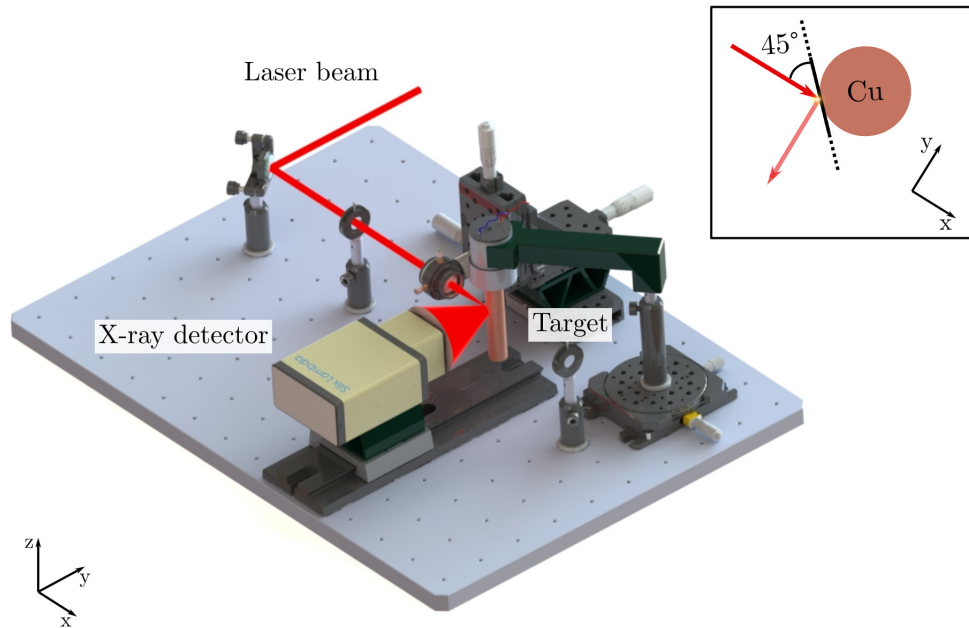


Fig. 1. Schematic of the experimental setup. An ultrafast laser beam is focused onto a copper cylinder target at an incidence angle of 45° , as shown schematically in the inset. A Silix Lambda spectrodosimeter is used to measure the dose rate and spectrum of the emitted X-ray radiation.

Table 1. List of used laser system and parameters

Laser	Wavelength	Repetition Rate	Pulse duration	Maximum power
CPA	800 nm	1 kHz	35 fs	1 W
OPCPA	800 nm	100 kHz	8 fs	6.5 W
Solid-state neoLASE	1030 nm	100 kHz	730 fs	60 W
SHG of neoLASE	515 nm	100 kHz	600 fs	30 W
Solid-state amplifier	1030 nm	1 MHz	850 fs	50 W

2.2. Spectrodosimeter

A calibrated Silix Lambda spectrodosimeter [32] is used as a detector to measure the spectrum and dose rate of the emitted X-ray simultaneously. The detectable spectral range covers from 1.78 to 20 keV with a spectral resolution of 0.24 ± 0.1 keV (FWHM) [33–35]. Figure 2 shows an example of X-ray spectrum from laser-induced plasma in solid copper obtained by using the OPCPA system presented in Table 1. A Bremsstrahlung continuum emission from about 2 to 7 keV is clearly visible. In addition, are also distinguishable K-shell lines contributions: a first narrow peak is visible around 8 keV corresponds to the K_α line of copper (8.046 keV), while a second weaker peak at 9 keV is near to the K_β line (8.904 keV) emission. With regards to the

dose rate, the Silix Lambda is capable to measure the ambient dose equivalent $H^*(10)$ and the directional dose equivalent $\dot{H}^*(0.07)$ simultaneously. Since the radiation investigated in this study is shallow penetrating, photon energy lower than 15 keV, only the equivalent dose rate $\dot{H}^*(0.07)$ is considered throughout the paper.

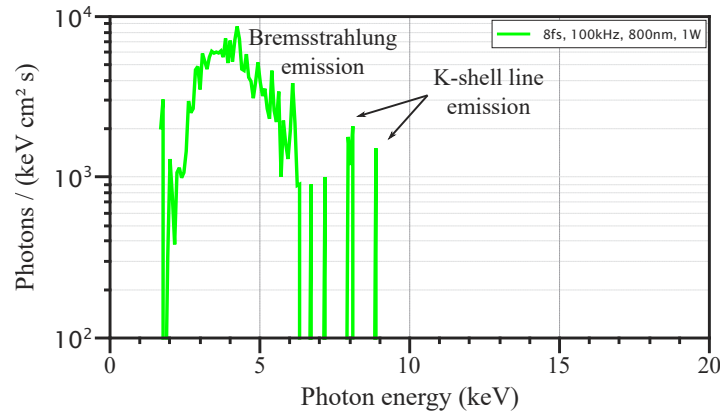


Fig. 2. X-ray spectrum from laser-induced plasma in a copper sample resolved with the spectrodosimeter Silix Lambda. The spectrum was obtained by using the OPCPA laser system (see Table 1) with an intensity of 10^{16} W/cm². Bremsstrahlung as well as k-shell line contributions are visible.

3. Results and discussions

3.1. Angular and distance analysis of X-ray dose rates

The measurement of dose rates is a fundamental practice for radiation protection, but neither the organ dose nor the effective dose can be measured directly. In order to estimate the radiation dose, conclusive models are essential. Typically, calibrated detectors are able to directly provide an estimation of the dose rate by applying several approximations, such as isotropic distribution of the X-ray radiation over a 4π solid angle. In contrast to X-ray tubes, the direction of the X-ray emission from laser-induced plasma is influenced by the local surface topography at the interaction spot, there the isotropic distribution approximation is not valid. For this reason, the analysis of the X-ray spatial distribution is necessary.

By using the experimental setup presented in Fig. 1, the angular dependence of the emitted radiation is measured by moving the X-ray detector around the interaction spot in 10° steps. The distance between the target and the detector is fixed at 100 mm. The distribution obtained is shown in Fig. 3(a). The angular distribution is clearly anisotropic with a maximum dose rate of $550 \mu\text{Sv/h}$ along the laser direction at an angle of 135° . Assuming a perfect cylindrical symmetry for the laser produced plasma, the dose rate emitted along the laser direction is expected to be similar to the one measured at 135° angle. However, this contribution cannot be measured without blocking the incoming laser beam and it is therefore shown as a dotted line in Fig. 3(a). This anisotropy of X-ray emission can be understood considering the effect of plasma opacity. For an optically thin plasma, the angular distribution is expected to be isotropic [32,36]. On the other hand, if the plasma is not optically thin, X-ray emission can be different for distinctive directions. The angular distribution of the X-ray emission from a plasma of certain volume and shape, would be governed by the optical depth faced by the radiation as it passing through the plasma [37,38]. The increasing thickness and density of the laser produced plasma leads to opacity effects, which strongly influence the anisotropy of the X-ray dose rate distribution [38].

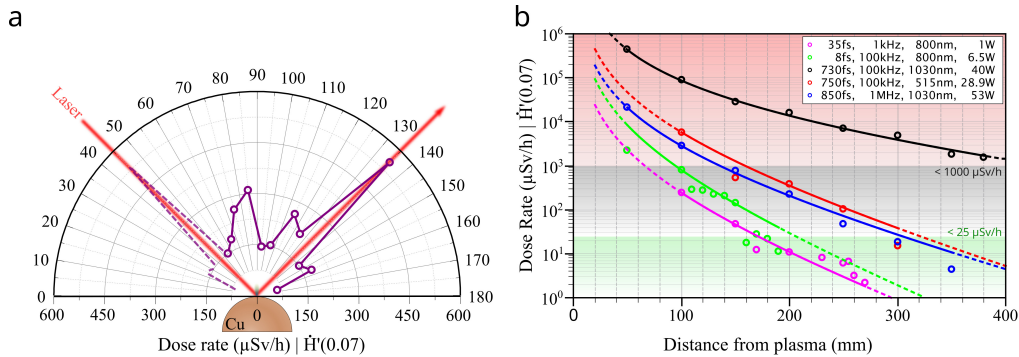


Fig. 3. (a) Dependence of X-ray dose rate on the detection angle, normal to the target surface, measured in air at a distance of 100 mm from the interaction zone. The measurements are performed with a laser intensity of about 10^{16} W/cm². (b) X-ray dose rates at varying distances from the interaction spot for different research grade laser systems. The lines represent a fit of the measured data, indicated by the circles. The limit values according to ICRP 103 for areas of continuous usage ($25 \mu\text{Sv/h} \mid \dot{H}'(0.07)$) and for temporary usage ($1000 \mu\text{Sv/h} \mid \dot{H}'(0.07)$) are marked.

A distance analysis is performed to complete the spatial distribution of the X-ray emission. The detector is placed at an angle of 135° (see Fig. 3(a)), where the maximum emission was previously found. The distance between the interaction spot and the detector is then varied from 50 to 350 mm in increments of 50 mm. For all laser systems, an exponential decrease of the dose rate with the distance from the interaction spot is observed, as shown in Fig. 3(b). This effect can be explained taking into consideration the absorption by air as well as the divergence of the X-ray radiation [39]. The predicted trend is shown by the continuous lines in Fig. 3(b). Note that, the presented calculations do not take in consideration the dependency of the absorption coefficient from the photon energy. This approximation is probably responsible from the small deviations of the experimental data from the calculated values at high photon energies. The rapidly decreasing trend in Fig. 3(b) is caused by absorption of low-energy photons. The longer the air distance, lesser photons with an energy < 6 keV reach the measurement sensor leading to a low measured value.

3.2. Dependency of X-ray dose rate on laser parameters

A comparison between the measured X-ray dose rate per pulse generated by the different laser systems is shown in Fig. 4. The laser intensity is varied in the range from 10^{13} to 10^{16} W/cm². It is evident that the X-ray dose rate follows an exponential increase up to a saturation regime. This behavior is expected due to the increasing conversion efficiency of X-ray generation with the laser intensity [40] until complete ionization of the material [24]. Note that the increase in X-ray dose rate can be either due to a higher X-ray photon counts or to the generation of X-ray with higher photon energy, or both. Depending on the laser system used, saturation occurs at different intensities. Since the measurements are all performed on the same material and geometry, this discrepancy must be due to the different laser parameters. In the following sections, the influence of four laser parameters are discussed: repetition rate, wavelength, pulse duration, and polarization.

Repetition rate. Previous studies has shown that the repetition rate is an important parameter for radiation safety during laser processing [23,25]. Depending on the processing parameters, such as velocity, line spacing, etc., repetition rates up to some hundreds of kHz can result in high dose per second. By comparing the dose per laser pulse, a different slope between the kHz and

the MHz range is clearly visible in Fig. 4. While there is no significant difference in the slope of the signal's increase with respect to the intensity I for the 1 kHz and the 100 kHz laser systems, the increase is much steeper in case of the 1 MHz system (blue curve in Fig. 4). The measured points were fitted with a function of the type:

$$D(I) = D_{sat} - \frac{D_{sat}}{1 + (I/I_{sat})^a} \quad (1)$$

where D_{sat} and I_{sat} are the X-ray dose and the laser intensity at the saturation level, respectively. The exponent a is found to be about 4 in case of kHz systems, while it is about 8 for the MHz laser system, indicating a different regime of interaction. In the MHz case, accumulation effects could be responsible for the different behaviour. For instance, a pulse can interact with the plasma generated from the previous one, leading to heating of the plasma and higher X-ray dose rate. Heat accumulation effects can also be present on the target surface, which is observed by the formation of molten material near the processed part. From a radiation safety point of view, it is then important to distinguish between laser systems with repetition rates up to a few hundreds of kHz) and higher, because pulse to pulse interaction can contribute to a higher total dose rate.

Laser wavelength. Another important parameter, which strongly influence the plasma evolution, is the laser wavelength. Following the ponderomotive law, longer driving wavelengths lead to an extended propagation of electrons in the plasma [13,41]. This results in emission of higher X-ray photon energies, which corresponds to an increase of the X-ray dose rate. The effect can be seen by comparing the X-ray spectra generated with different driving wavelength, as shown in Fig. 5. Here, a broader Bremsstrahlung continuum up to 15 keV is detected for the 1030 nm solid-state neoLASE laser system (black curve) compared to a maximum of 7 keV generated with the 515 nm SHG of the solid-state neoLASE system (red curve). Note that the X-ray spectrum for the solid-state amplifier (blue curve) includes only Bremsstrahlung emission due to, as already mention, the pulse-to-pulse interactions, which leads to heat accumulation, molten material and emitted sparks. When higher X-ray photon energies are generated, a higher saturation point for the X-ray dose rate per pulse is expected. This effect is clearly visible in Fig. 4 comparing again the 1030 nm system (black curve) to the 515 nm one (red curve).

Pulse duration. With very short pulses of a few fs, the maximum X-ray radiation per pulse is expected to be significantly lower compared to longer pulse durations. This can be explained by the fact that a very fast and very strong laser field results in a quick deposition of energy in the material and short plasma lifetime. Moreover, since the laser pulse ends in the early stage of the plasma formation, it cannot additionally contribute to the plasma heating. As a consequence, the maximum X-ray dose per pulse is expected to be lower compared to longer pulse durations. By comparing the 8 fs OPCPA (green curve) laser system and the 35 fs CPA (purple curve) in Fig. 4, the X-ray dose rate per pulse is indeed found to be around 100-times lower for the shorter pulse duration. Note that this decrease cannot be explained only by the difference in pulse energy (maximum 65 μJ / intensity for the OPCPA and 1 μJ for the CPA laser system). An even more clear influence is visible when comparing the X-ray dose over time, shown in Fig. 6. With the 8 fs OPCPA laser system, the X-ray dose decreases in a short time (less than one minute) as the material is ablated. While for longer laser pulse durations the X-ray dose rate persists over time with a change of the X-ray spectrum to pure Bremsstrahlung, without line emission.

A similar trend is also evident when comparing the 35 fs CPA laser system (purple curve) with the longer pulse duration provided by the solid-state neoLASE (black curve) and the solid-state amplifier (blue curve), indicating a different regime between ultrashort pulses of a few fs duration and comparatively longer pulses. Therefore, from a safety point of view, laser systems with pulse duration of hundreds of fs can lead to a stronger X-ray dose rate and therefore require stronger radiation protective measures with respect to shorter pulses.

Polarization. Another interesting aspect is the higher X-ray dose rate measured for p-polarized laser light compared to s-polarized light, while other parameters are kept constant. As shown in

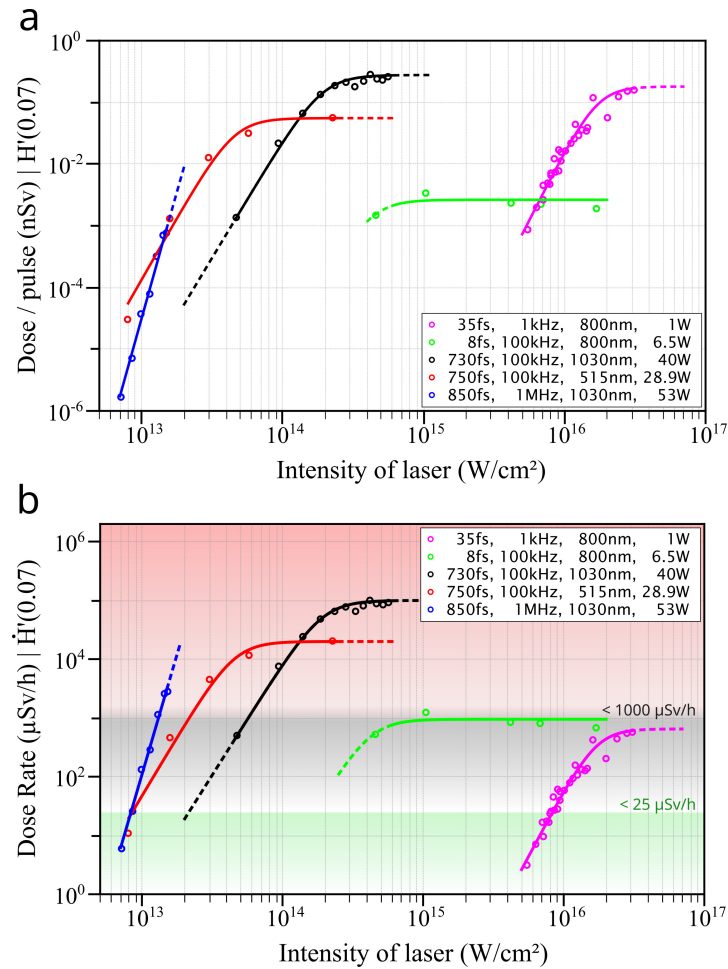


Fig. 4. (a) Measured dose $\dot{H}'(0.07)$ per laser pulse as a function of intensity for different research grade lasers. The dose per pulse increases exponentially up to saturation. The lines represent a fit of the measured data, which are indicated by the circles. (b) Measured dose rate $\dot{H}'(0.07)$ per hour as a function of intensity. The limit values according to ICRP 103 for areas of continuous usage ($25 \mu\text{Sv/h} | \dot{H}'(0.07)$) and for temporary usage ($1000 \mu\text{Sv/h} | \dot{H}'(0.07)$) are marked.

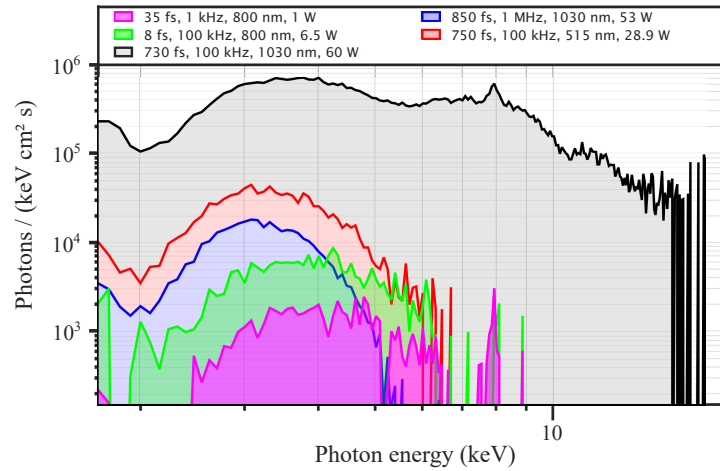


Fig. 5. Normalized X-ray spectrum from a copper cylinder target for different research grade laser systems at their maximum intensity (see Table 1).

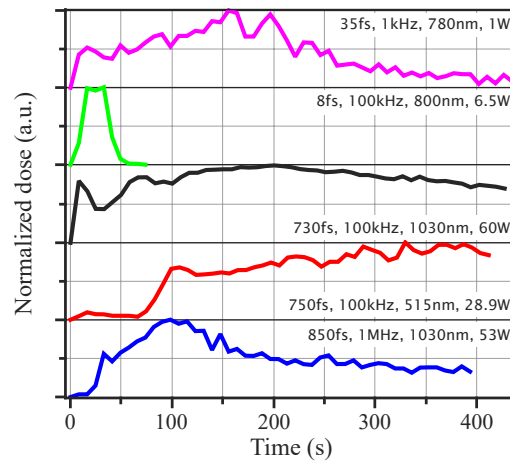


Fig. 6. Normalized X-ray dose rate $\dot{H}'(0.07)$ recorded for different research grade laser systems as function of time at their maximum intensity (see Table 1). The measurement starts at time zero, when the laser interaction with the target starts, and it lasts about 400 seconds.

Fig. 7, the measured X-ray dose rate decreases to about half when the laser beam polarization is changed from horizontal to vertical, i.e. p to s-polarization with respect to the target. For the CPA laser system, the maximum X-ray dose rate of $550 \mu\text{Sv/h}$ for p-polarized light is reduced to $350 \mu\text{Sv/h}$ when it is changed to s-polarization. These observations are in agreement with other previous publications [23,42]. The effect is commonly attributed to resonance absorption that, at high intensities ($>10^{15} \text{ W/cm}^2$), can lead to a plasma profile steepening and localized electron plasma oscillations, which are a source for hot electrons [23,43]. The p-polarized light resonantly excites these electron plasma oscillations which may lead to a higher X-ray dose rate. In the case of s-polarized light, the energy of the laser field is not resonantly coupled to the electron-plasma wave. So, the absence of resonance absorption for the s-polarized laser light leads to the overall difference in X-ray dose rate.

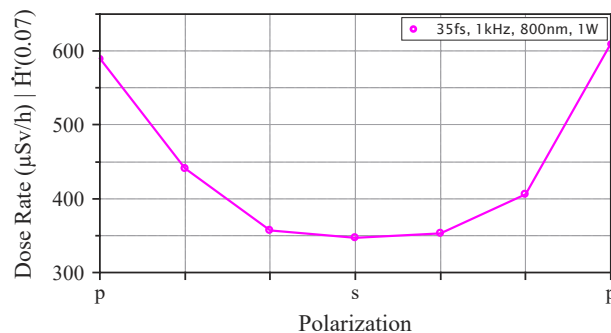


Fig. 7. Measured X-ray dose rate $\dot{H}'(0.07)$ with respect to laser polarization for the CPA laser system at an intensity of about 10^{16} W/cm^2 .

3.3. Measurements of the X-ray dose for an in-situ case

Potential radiation hazards are not limited to the laser produced plasma from solid targets, but can be present also for a wide range of laser-matter interactions. As already shown in Fig. 4, X-ray emission can be generated with intensity even below 10^{13} W/cm^2 . In typical research grade laser systems, this intensity range can be reached i.e., for supercontinuum or harmonic generation in solid material. Here we present an example of white-light generation using the solid-state amplifier (see Table 1) inside a home-built ultrashort laser system. The white-light generation takes place in a 5 mm Yttrium-Aluminum-Garnet (YAG) crystal using a $f = 30 \text{ mm}$ planoconvex lens reaching an intensity of $6 \times 10^{12} \text{ W/cm}^2$ in the focus. Characteristic line emission of Yttrium were clearly detected around 15 keV with an X-ray dose rate of $0.66 \mu\text{Sv/h}$, which corresponds to six times the background radiation. According to the German Radiation Protection Ordinance no regulations are foreseen as long as 10^{13} W/cm^2 are not exceeded and the X-ray dose rate is limited to $1 \mu\text{Sv/h}$ maximum. But the presented example indicates that potential hazardous X-ray emission can also be observed during normal operation of high intensity lasers and should be considered for radiation protection. Detailed in-situ measurements are under investigation which will be presented in future publications.

3.4. Dose rate and spectrum for different shielding materials

The hands and eyes of experimentalists are at particularly risk of exposure from X-ray radiation during laboratory work. As already mentioned, the recommended annual dose equivalent limit set by the ICRP is 15 mSv/year ($\dot{H}'(3)$) for the eye and 50 mSv/year ($\dot{H}'(0.07)$) for skin and extremities., while the legal annual effective dose limit value for the general population in Germany is 1 mSv $\dot{H}'(10)$ [44]. As shown previously, laser-matter interaction, even at relatively

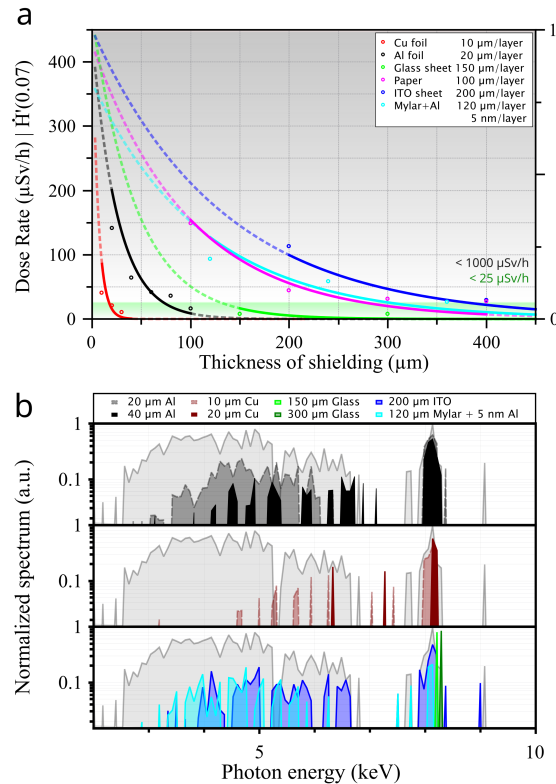


Fig. 8. (a) Dose rate $\dot{H}'(0.07)$ dependence with respect to the thickness of different shielding materials. The measurement is performed at a distance of 100 mm from the laser interaction spot. The measurement is carried out with the CPA laser system, with an intensity of about 10^{16} W/cm^2 on the copper target. The limit values according to ICRP 103 for areas of continuous usage ($25 \mu\text{Sv/h} \mid \dot{H}'(0.07)$) and for temporary usage ($1000 \mu\text{Sv/h} \mid \dot{H}'(0.07)$) are marked. (b) Corresponding attenuated X-ray spectrum for the different shielding materials.

low laser intensities, can lead to exposures which exceed this statutory limit. In this scenario, radiation protection from X-ray radiation is of fundamental importance not only in the field of laser machining industries, but also in research laboratories. When a high-intensity laser-matter interaction experiment is carried out in vacuum, the vacuum chamber itself serves as the primary shielding for the generated X-ray radiation. The walls of the chamber are usually made of aluminum or stainless steel providing good shielding properties [22,45,46]. It is well known that steel is a widely used protective material but it cannot be used in all cases in a research laboratory. However, even in this case, glass viewports are often used and can allow propagation of very high energetic radiation ($>20 \text{ keV}$), requiring additional shielding. Moreover, we have shown a specific case in which the X-ray radiation was generated inside a high-power laser system. Investigation of potential radiation hazards should not be disregarded and suitable shielding material must be used.

Figure 8 shows the thickness dependence and attenuation of different protective materials on the X-ray dose rate and spectrum. All tested materials are inexpensive and can be quickly assembled as a protective housing. A solution for lead-free and easily assembled X-ray photon shielding is always of interest to the scientific community [47]. In the soft X-ray range copper and aluminium sheets can provide efficient shielding [33]. Copper foil is highly efficient in eliminating the

Bremsstrahlung X-ray continuum while providing high transmission of the characteristic X-ray line emission. ITO and Mylar foils reduce the X-ray dose rate only above a greater thickness (> 0.1 mm), while reducing the spectrum homogeneously, making them a good filter material often used to reduce the pile-up in X-ray detectors. Based on the spectral measurements, we found that glass suppresses Bremsstrahlung very efficiently. Moreover, to avoid X-ray fluorescence, a plastic layer should be used before the metal layer. Therefore the most suitable shielding material should then be chosen accordingly to the specific application.

4. Conclusions

A dependency between the laser parameters and the generation of X-ray radiation as well as the possibilities for mitigating the X-ray dose rate for practical radiation protection are given. The spatial distribution analysis showed an anisotropic X-ray emission, clearly peaked along the direction of the laser and with a gradual decrease with increasing distance from the generation spot. Moreover, harmful X-ray emission can already occur at laser intensities of 10^{13} W/cm². It is therefore advisable to identify the X-ray dose rate at every laser-material interaction spot. The absorption measurement points out how important it is to know the emitted X-ray spectrum in order to use appropriate shielding. In any case, the safe distance should be determined according to the laser parameters, as it depends on both the laser parameters and the properties of the target material. Additional thin sheets of aluminum or copper could be used as an efficient protective shielding from X-ray radiation.

Funding. HORIZON EUROPE European Innovation Council (EIC Open grant No. 101047223-NanoXCAN); Deutsche Forschungsgemeinschaft (EXC 2122, EXC-2123, PhoenixD - 390833453, Quantum Frontiers - 390837967).

Acknowledgments. Funded by the Deutsche Forschungsgemeinschaft (DFG, German Research Foundation) under Germany's Excellence Strategy within the Cluster of Excellence PhoenixD (EXC 2122, Project ID 390833453) and EXC-2123 Quantum Frontiers - 390837967, EIC Open grant No. 101047223-NanoXCAN.

Disclosures. The authors declare no conflicts of interest.

Data availability. Data underlying the results presented in this paper are not publicly available at this time but may be obtained from the authors upon reasonable request.

References

1. G. Kamlage, T. Bauer, A. Ostendorf, and B. Chichkov, "Deep drilling of metals by femtosecond laser pulses," *Appl. Phys. A* **77**(2), 307–310 (2003).
2. F. A. Müller, C. Kunz, and S. Gräf, "Bio-inspired functional surfaces based on laser-induced periodic surface structures," *Materials* **9**(6), 476 (2016).
3. J. Schille, L. Schneider, S. Mauersberger, S. Szokup, S. Höhn, J. Pötschke, F. Reiß, E. Leidich, and U. Löschner, "High-Rate Laser Surface Texturing for Advanced Tribological Functionality," *Lubricants* **8**(3), 33 (2020).
4. M. Gafner, T. Kramer, S. M. Remund, R. Holtz, and B. Neuenschwander, "Ultrafast pulsed laser high precision micromachining of rotational symmetric parts," *J. Laser Appl.* **33**(1), 012053 (2021).
5. A. B. Kaligar, H. A. Kumar, A. Ali, W. Abuzaid, M. Egilmez, M. Alkhader, F. Abed, and A. S. Alnaser, "Femtosecond laser-based additive manufacturing: Current status and perspectives," *Quantum Beam Sci.* **6**(1), 5 (2022).
6. H. Huang, B. Nie, P. Wan, L.-M. Yang, S. Bai, and J. Liu, "Femtosecond fiber laser additive manufacturing and welding for 3D manufacturing," in *Laser 3D Manufacturing II*, vol. 9353 (SPIE, 2015) pp. 28–39.
7. D. Bäuerle, "Nanosecond-laser ablation," in *Laser Processing and Chemistry* (Springer, 2011) pp. 237–278.
8. J. Thogersen, A. Borowiec, H. Haugen, F. McNeill, and I. Stronach, "X-ray emission from femtosecond laser micromachining," *Appl. Phys. A* **73**(3), 361–363 (2001).
9. J. Bunte, S. Barcikowski, T. Puester, T. Burmester, M. Brose, and T. Ludwig, "Secondary hazards: Particle and x-ray emission," *Femtosecond Technol. for Tech. Med. Appl.* **96**, 309–321 (2004).
10. B. Hou, J. Easter, K. Krushelnick, and J. A. Nees, "Generation of hard x rays by femtosecond laser pulse interaction with Cu in laminar helium flow in ambient air," *Appl. Phys. Lett.* **92**(16), 161501 (2008).
11. R. Behrens, B. Pullner, and M. Reginatto, "X-Ray emission from materials processing lasers," *Radiat. Prot. Dosim.* **183**(3), 361–374 (2018).
12. F. F. Chen, *Introduction to Plasma Physics and Controlled Fusion*, 3rd ed. (Springer, 2016).
13. P. Gibbon and E. Förster, "Short-pulse laser-plasma interactions," *Plasma Phys. Controlled Fusion* **38**(6), 769–793 (1996).
14. B. Luther-Davies, "X-ray bremsstrahlung and fast-ion measurements from picosecond laser-produced plasmas," *Opt. Commun.* **23**(1), 98–104 (1977).

15. G. Enright, M. Richardson, and N. Burnett, "Superthermal x-ray emission from co₂-laser-produced plasmas," *J. Appl. Phys.* **50**(6), 3909–3914 (1979).
16. W. Chao, B. D. Harteneck, J. A. Liddle, E. H. Anderson, and D. T. Attwood, "Soft x-ray microscopy at a spatial resolution better than 15 nm," *Nature* **435**(7046), 1210–1213 (2005).
17. L. Miaja-Avila, G. C. O'Neil, J. Uhlig, C. L. Cromer, M. L. Dowell, R. Jimenez, A. Hoover, K. L. Silverman, and J. N. Ullom, "Laser plasma x-ray source for ultrafast time-resolved x-ray absorption spectroscopy," *Struct. Dyn.* **2**(2), 024301 (2015).
18. D. Umstadter, "Review of physics and applications of relativistic plasmas driven by ultra-intense lasers," *Phys. Plasmas* **8**(5), 1774–1785 (2001).
19. F. Barbato, D. Scarpellini, A. Malizia, P. Gaudio, M. Richetta, and L. Antonelli, "X-ray high-resolution spectroscopy for laser-produced plasma," *Phys. Procedia* **62**, 84–91 (2015).
20. M. Cavallone, L. Rovige, J. Huijts, É. Bayart, R. Delorme, A. Vernier, P. G. Jorge, R. Moeckli, E. Deutsch, J. Faure, and A. Flacco, "Dosimetric characterisation and application to radiation biology of a khz laser-driven electron beam," *Appl. Phys. B* **127**(4), 57 (2021).
21. M. Afshari, P. Krumei, D. Menn, M. Nicoul, F. Brinks, A. Tarasevitch, and K. Sokolowski-Tinten, "Time-resolved diffraction with an optimized short pulse laser plasma x-ray source," *Struct. Dyn.* **7**(1), 014301 (2020).
22. H. Legall, C. Schwanke, S. Pentzien, G. Dittmar, J. Bonse, and J. Krüger, "X-ray emission as a potential hazard during ultrashort pulse laser material processing," *Appl. Phys. A* **124**(6), 407 (2018).
23. H. Legall, C. Schwanke, J. Bonse, and J. Krüger, "The influence of processing parameters on x-ray emission during ultra-short pulse laser machining," *Appl. Phys. A* **125**(8), 570 (2019).
24. R. Weber, R. Giedl-Wagner, D. J. Förster, A. Pauli, T. Graf, and J. E. Balmer, "Expected x-ray dose rates resulting from industrial ultrafast laser applications," *Appl. Phys. A* **125**(9), 635 (2019).
25. H. Legall, J. Bonse, and J. Krüger, "Review of x-ray exposure and safety issues arising from ultra-short pulse laser material processing," *J. Radiol. Prot.* **41**(1), R28–R42 (2021).
26. J. Schille, S. Kraft, T. Pflug, C. Scholz, M. Clair, A. Horn, and U. Loeschner, "Study on x-ray emission using ultrashort pulsed lasers in materials processing," *Materials* **14**(16), 4537 (2021).
27. S. Vallières, J. Powell, T. Connell, M. Evans, S. Fourmaux, S. Payeur, P. Lassonde, F. Fillion-Gourdeau, S. MacLean, and F. Légaré, "High dose-rate ionizing radiation source from tight focusing in air of a mj-class femtosecond laser," arXiv:2207.05773 (2022).
28. B. Hou, J. A. Nees, W. Theobald, G. A. Mourou, L. Chen, J.-C. Kieffer, A. Krol, and C. Chamberlain, "Dependence of hard x-ray yield on laser pulse parameters in the wavelength-cubed regime," *Appl. Phys. Lett.* **84**(13), 2259–2261 (2004).
29. T. Zhao, T. Batson, B. Hou, J. Nees, A. Thomas, and K. Krushelnick, "Characterization of hard x-ray sources produced via the interaction of relativistic femtosecond laser pulses with metallic targets," *Appl. Phys. B* **125**(1), 8–9 (2019).
30. ICRP, "Recommendations of the International Commission on Radiological Protection," ICRP Publication 103, Ann. ICRP 37 (2–4) (2007).
31. J. H. Kim, "Three principles for radiation safety: time, distance, and shielding," *The Korean journal of pain* **31**(3), 145–146 (2018).
32. P. Mosel, P. Sankar, J. F. Düsing, G. Dittmar, T. Püster, P. Jäschke, J.-W. Vahlbruch, U. Morgner, and M. Kovacev, "X-ray dose rate and spectral measurements during ultrafast laser machining using a calibrated (high-sensitivity) novel x-ray detector," *Materials* **14**(16), 4397 (2021).
33. U. Stolzenberg, M. Schmitt Rahner, B. Pullner, H. Legall, J. Bonse, M. Kluge, A. Ortner, B. Hoppe, and J. Krüger, "X-ray emission hazards from ultrashort pulsed laser material processing in an industrial setting," *Materials* **14**(23), 7163 (2021).
34. G. Dittmar and J. Nolting, "Aus der praxis: Überwachung der röntgenemission bei ultrakurzpuls-lasern," *sicher ist sicher* (2021).
35. G. Dittmar, "Neue Messtechnik für die 'Laserinduzierte Ionisierende Strahlung' bei Ultrakurzpulslasern?" *Strahlenschutzpraxis* 27–2021, 23–28 (2021).
36. J. Broughton and R. Fedosejevs, "keV x-ray production using 50 mJ krf laser produced plasmas at 1 and 100 ps," *J. Appl. Phys.* **74**(6), 3712–3723 (1993).
37. B. Rao, P. Naik, V. Arora, R. Khan, and P. Gupta, "Angular distribution and dose measurements of hard x-ray emission from intense laser-plasma interaction," *J. Appl. Phys.* **102**(6), 063307 (2007).
38. V. Arora, J. Chakera, S. Kumbhare, P. Naik, N. Gupta, and P. Gupta, "Angular distribution of x-ray line radiation from laser-irradiated planar targets," *Laser Part. Beams* **19**(2), 253–257 (2001).
39. F. H. Day and L. S. Taylor, "Absorption of x-rays in air," *Radiology* **52**(2), 239–247 (1949).
40. I. Toubhans, R. Fabbro, J. Gauthier, M. Chaker, and H. Pepin, "X-ray conversion efficiency in laser-produced plasmas. application to x-ray lithography," in *X-Ray Instrumentation in Medicine and Biology, Plasma Physics, Astrophysics, and Synchrotron Radiation*, vol. 1140 (International Society for Optics and Photonics, 1989) pp. 358–366.
41. D. Forslund, J. Kindel, and K. Lee, "Theory of hot-electron spectra at high laser intensity," *Phys. Rev. Lett.* **39**(5), 284–288 (1977).
42. W. Krueer, *The Physics of Laser Plasma Interactions* (CRC Press, 2019).

43. U. Teubner, J. Bergmann, B. Van Wonterghem, F. Schäfer, and R. Sauerbrey, "Angle-dependent x-ray emission and resonance absorption in a laser-produced plasma generated by a high intensity ultrashort pulse," *Phys. Rev. Lett.* **70**(6), 794–797 (1993).
44. "Bfs - startseite," https://www.bfs.de/DE/home/home_node.html. Accessed: 2022-03-01.
45. B. R. Archer, T. R. Fewell, B. J. Conway, and P. W. Quinn, "Attenuation properties of diagnostic x-ray shielding materials," *Med. Phys.* **21**(9), 1499–1507 (1994).
46. M. A. B. Aziz, M. F. Rahman, and M. M. H. Prodhan, "Comparison of lead, copper and aluminium as gamma radiation shielding material through experimental measurements and simulation using mcnp version 4c," *Int. J. Cont. Res. Rev.* **9**(08), 20193–20206 (2018).
47. Z. Li, W. Zhou, X. Zhang, Y. Gao, and S. Guo, "High-efficiency, flexibility and lead-free x-ray shielding multilayered polymer composites: layered structure design and shielding mechanism," *Sci. Rep.* **11**, 1–13 (2021).